Fisheries Research xxx (2016) xxx–xxx

Contents lists available at ScienceDirect

Fisheries Research

journal homepage: www.elsevier.com/locate/fishres

Full length article

3D-Xray-tomography of American lobster shell-structure. An overview

Joseph G. Kunkel[a,b,*], Melissa Rosa[b], Ali N. Bahadur[c]

[a] University of Massachusetts, Amherst, MA 01003, United States
[b] University of New England, Biddeford, ME 04005, United States
[c] Bruker BioSpin Corp., Billerica, MA 01821, United States

ARTICLE INFO

Article history:
Received 16 January 2016
Received in revised form
13 September 2016
Accepted 23 September 2016
Available online xxx

Keywords:
Homarus americanus
American lobster
MicroCT
Xray tomography
Organule
Cuticle
Structure
Bouligand layers

ABSTRACT

A total inventory of density defined objects of American lobster cuticle was obtained by using high resolution 3D Xray tomography, micro-computed-tomography. Through this relatively unbiased sampling approach several new objects were discovered in intermolt cuticle of the lobster carapace. Using free and open-source software the outlines of density-defined objects were obtained and their locations in 3D space calculated allowing population parameters about these objects to be determined. Nearest neighbor distances between objects allowed interpretations of structural relationships of and between objects. Several organule types are recognized by their structural outlines and density signatures. A hierarchy of organule types and distribution suggests they develop during sequential molts. New objects (stalactites, Bouligand spirals, and basal granules) are described as mineral structures with well defined morphological character, allowing them to be recognized by their descriptive names and distributions. The three new cuticular objects appear to represent forms of calcium carbonate deposition in the sequential layers of exocuticle, endocuticle and membranous layer and may provide signatures of underlying epidermal cells.

1. Introduction

Research on American Lobster, *Homarus americanus*, cuticle continues to be of interest to material scientists as a composite material, to immunologists as an antigen and to pathologists as the target of shell disease. The current chemical and physical models of arthropod cuticle are based on a long standing interest in modeling the LM, TEM and SEM views of cuticle structure as well as the chemistries of chitin (Richards, 1951), protein polymer and small molecules (Andersen, 2010) in cuticle structure. The primary breakthrough in understanding the apparent layers of the cuticle was made when the illusion of layering was explained as a more gradual rotation of the angle of orientation of chitin fibers in the plane of the cuticle (Bouligand, 1972). When the angle of layered fibers rotates through 180° there is an illusion of a layer in the cuticle. Additional interest has developed in designing biopolymers as biomimetic composite materials (Fabritius et al., 2009; Nikolov et al., 2011), applying engineering principles to understand structural properties (Raabe et al., 2006; Romano et al., 2007; Grunenfelder et al., 2014) associated with the Bouligand (1972) layers of so-called twisted-fiber plywood structure of the cuticle. The structure of lobster cuticle is informed by knowledge of the chitin and protein polymers associated with particular cuticle layers (Kunkel, 2013) and the organic chemistry associated with hardening or flexibility after molting (Andersen, 2010). Departures from the uniform structure of the cuticle exemplified in various Decapod cuticles by regular surface sculpturing, including but not limited to organule

Abbreviations: AFM, atomic force microscopy; AVI, a digital movie file type produced by ImageJ image analysis software; CSV, comma-separated-value type text file is a widely used non-proprietory rectangular data file used to transfer data between software applications; EMP, electron microprobe; ESD, epizootic shell disease is a locally prevalent disease (currently of unknown cause) in natural populations of American lobster differing (in its striking abundance) from endemic shell disease which is found at very low levels in all lobster populations (Smolowitz et al. 2005); FTIR, fourier transform infrared analysis; LM, light microscopy; microCT, micro computed tomography; NA, a reserved word in the R language referring to a missing value; NND, nearest neighbor distance. NND is the euclidean distance of an object centroid to its nearest neighbor's centroid; R, R is a General Public License (GNU) computation environment open-source programming and graphical tool; R rgl, the rgl library is a downloadable add on to R that allows creating 3D rotatable plotting spaces with functions for using those spaces to create plane views stereo views and movies; SEM, scanning electron microscopy; TEM, transmission electron microscopy; μm, micrometer 10^{-6} meters; voxel, the building block of 3D-arrays making up a solid structure; XRT, Xray tomography.

* Corresponding author at: Bickford St., Scarborough, ME 04074, United States.
E-mail addresses: joe@bio.umass.edu, jkunkel1@une.edu, joe@bio.umass.edu12 (J.G. Kunkel).

http://dx.doi.org/10.1016/j.fishres.2016.09.028
0165-7836/

structures, have been implicated in avoiding structural failure of the cuticle (Tarsitano et al., 2006).

Earlier models of cuticle structure are based on one dimensional analysis of powdered cuticle, e.g. X-ray powder pattern analysis (Lowenstam 1981; Lowenstam and Weiner, 1989) or various two dimensional analyses of sections of de-mineralized cuticle (Smolowitz et al., 2005) or polished surfaces of mineralized cuticle (Hayes and Armstrong, 1961; Fabritius et al., 2009; Kunkel et al., 2012; Kunkel and Jercinovic, 2013; Kunkel 2013) that derive their interpretations from one or two-dimensional data analysis.

One dimensional studies (e.g. chemical analysis of whole cuticle) are biased by focusing on average compositions, ignoring the importance of the abundant but small regular features, such as the organules, which are developmentally related small secretory and sensory organs, first described in insects but present in all arthropods. Most two dimensional studies of biological structure (e.g. AFM, LM, TEM, SEM, EMP, micro Raman and micro FTIR) are biased by investigator selection of ideal views of successful sections or polished surfaces which are more immediately interpretable. Often one sees a small sample of the possible sections, others being rejected as being not representative or not easily fit into a general model. Investigators interested in modeling 'general' cuticle properties have often avoided considering organule structures, e.g. the dermal gland canals and sensory bristles, in their models as being beyond the current level of interest and in hope of reaching an *ab initio* model of the composite material nature of cuticle (Raabe et al., 2006; Fabritius et al., 2009; Nikolov et al., 2011). These one- and two-dimensional studies may not represent an exhaustive or accurate window into the diversity, physical relationships or importance of cuticle structures. Since the available chemical analytical and structural data on lobster cuticle, obtained by one- and two-dimensional studies, does not show the 3D view of the micro-architecture of the cuticle, we implemented a three dimensional study of lobster cuticle based on the density of the cuticle to X-rays using the recently available high resolution X-ray computed tomography or microCT (Naleway et al., 2016). Resultant voxel density data derived from a limited number of lobsters sampled is immense and allows for cataloging all structures observable at the resolution of the technique. Here our immediate focus is to provide an overview of new objects discovered in carapace cuticle by focusing on micro density measurements. The relationships of these new objects with historically described cuticle structures are described, particularly with the developmentally important layers: epicuticle, exocuticle, endocuticle and membranous layer (Bouligand 1972; Waddy et al., 1995), and with the carapace organules (Henke, 1952; Merritt, 2006; Kunkel, 2013).

2. Materials and methods

2.1. Animals

The American lobster cuticles in this study were obtained from specimens collected Spring 2009 during leg three of a Northeast Groundfish Survey of NOAA Ship HB Bigelow on the outer (eastern edge) of Georges Bank in USA territorial waters, which is effectively the eastern edge of the Northeast USA continental shelf. This offshore population of American lobsters sampled was historically free of epizootic shell disease (ESD) (Glenn and Pugh, 2006) and the samples reported on here are considered to be from normal lobsters recently taken from nature. All lobsters were intermolt, stage C4, which is a holding stage before induction of the next molting cycle (Waddy et al., 1995). Sections of medial lateral carapace cuticle (1.5 × 3 cm) were excised from euthanized lobsters and fixed in 50 ml of −40 °C 95% ethyl alcohol, changed twice over 24 h, and subsequently stored in absolute alcohol. The sampled piece of cuticle is biased in avoiding the major suture lines and muscle insertions and apodemes of the carapace, but is unbiased in recording all the density defined objects including the pattern of exoskeleton organules as previously described (Kunkel and Jercinovic, 2013) for the primary site of ESD.

2.2. Cuticle medallion preparation

A drill press with coring drill bit was used to obtain 6 mm medallions of cuticle from dorsal lateral carapace pieces stored in absolute alcohol. Medallions were air dried overnight and attached with Super-Glue® to a 25 mm resin block in triangular arrays for stability while grinding. The triads of medallions were briefly ground with a carborundum disc (600 grit) at high speed on a rotary wheel to approximate desired depth. They were then finely polished with a no-nap lapping cloth (Trident ™) with 6, 3, 1, 0.25 μm diamond (Buehler, Metadi Supreme®) in lapping oil. They were cleaned after each polishing level with anhydrous solvents (100% isopropyl alcohol and 100% acetone recently treated with Molecular Sieve (Sigma-Aldrich) to scavenge water) to remove grinding media and oil. These samples were objects further processed for EMP (Kunkel et al., 2005), microRaman, microFTIR and microCT analysis to characterize structures at various levels in the cuticle.

2.3. MicroCT

Micro-computed-tomography (microCT) scans were performed using the Skyscan 1272 (Bruker MicroCT, Kontich, BE), a high resolution desktop microCT scanner for specimen imaging. The system is capable of scanning samples at resolutions as high as 0.35 μms. All samples (M1C, M2C and M3A, Supplementary Table S1) were portions of 6 mm diameter medallions and scanned at 3.5 μm (low resolution) isotropic voxel resolution, with the x-ray voltage at 40 kV and x-ray current at 222 μA using the 0.25 mm Aluminum filter. The raw acquisitions were collected every 0.2 rotational degree with a 1150 ms exposure time for each image. Sample M3A was scanned at 1.5 μm (high resolution) isotropic voxel resolution, 40 kV x-ray voltage, 222 μA x-ray current and 0.25 mm Aluminum filter. The raw acquisitions were collected every 0.2 rotational degree with a 1900 ms exposure time for each image. Sample M2C was scanned at 0.5 μm (highest resolution) isotropic voxel resolution, 40 kV x-ray voltage, 222 μA x-ray current and 0.25 mm Aluminum filter. The raw acquisitions were collected every 0.1 rotational degree with a 3800 ms exposure time for each image. The raw acquisitions were reconstructed to axial cross-sectional slices using Nrecon (ver 1.6.9.8) using standard parameters to generate 3Dimensional grayscale images. All datasets were further reoriented and cropped to smaller regions using DataViewer (ver 1.5.1.2). Since creating outlines of linear structures is difficult when they are not orthogonal to a current axis, it was of particular use to rotate long structures such as canals so that their new orientation was perpendicular to a new voxel plane before extracting their contours.

2.4. Software

Several software packages were essential to this study and were non-proprietary or freely available. Data from the microCT data processed by Nrecon exists as individual 2D slices in typical lossless BMP, TIF formats. A lossless storage of pixel values is necessary for quantitative measurements on the data. DataViewer (available at http://bruker-microct.com/products/downloads.htm) is essential for rotating and subsetting the huge number of voxels in the available 2D sliced files into smaller prismatic assemblages of voxels as a smaller or reoriented set of 2D slices that contain a structural object of interest. These subset slices can be accessed by ImageJ (the

Please cite this article in press as: Kunkel, J.G., et al., 3D-Xray-tomography of American lobster shell-structure. An overview. Fish. Res. (2016), http://dx.doi.org/10.1016/j.fishres.2016.09.028

cross-platform public domain software developed from NIH Image) and stored in a smaller lossy (JPEG) or lossless but larger (TIFF or PNG) single file or AVI movie format which can be processed in ImageJ in multiple ways but here primarily to create xyz-coordinate outlines of the density defined objects provided by microCT. The derived outline coordinates were exported as CSV files. The CSV files were read by the R function read.csv and the x, y and z coordinates used to draw outlines in 3D using the R rgl library of functions.

2.5. Data processing

Rotated and cropped rectangular prisms of density voxels spanning a structure of interest were written via ImageJ as 3 orthogonal AVI files, one with layers of voxels in the XY-plane, one in the XZ-plane and one in the YZ-plane using DataViewer. To obtain contours in particular planes an AVI was read into ImageJ, an interpretive color Lookup Table (LUT) chosen and contours of features located and recorded with the pointing tool after setting the scale with appropriate μm per voxel edge. In ImageJ, contours were defined by choosing a series of points on the outline of the object in an initial section of voxels, and when the choice was completed in that section, the point-choice was allowed to continue in adjacent z-dimension sections without punctuation; but, when an interruption was appropriate (such as when a 3D object's contour was completed), a point close to (x y)=(0 0) of the current section was collected with the pointing tool and in a subsequent pre-analysis step all such (x y)-near zero points were turned into missing value symbols (NA) in the data file. In this way data representing closed-figures in the x-, y- and z-dimensions could be defined as those between NAs. Collecting orthogonal contours for the same objects helped to visualize the objects in 3D particularly during rotation. Completing two or three of the orthogonal contours for a given object was facilitated by plotting all contours collected by a given time, plotting them in an R rgl 3D window, and seeing if orthogonal contours were missing from particular objects. The files of similar closed figure contours were saved together as single CSV files for that object type and thus could be plotted with an appropriate color based on the file id. CSV files were accessed to create graphical objects in 3D using the R computation environment with the required rgl library. Where appropriate, the centroids of closed figure objects (such as organule pits, granules or stalactites) were calculated in R and nearest neighbor distance (Clark and Evans, 1954) analysis done on a collection of objects using custom R-scripts. The 3D rendering of objects used scripts allowing assignment of color, thickness and transparency to structures, rotating them and writing them to PNG files using the movie3D function of the R rgl library. In turn the series of PNG files output from movie3D were imported into ImageJ, cropped to appropriate limits and saved as a smaller JPEG compression AVI movie.

3. Results

3.1. Sample resolution

All three lobster samples were scanned at the lower resolution, 3.5 μm/voxel edge. Two other scan resolutions were applied, the highest resolution 0.5 μm/voxel to sample M2C and 1.5 μm/voxel to sample M3A. Each resolution was evaluated for its benefits. Feature properties were investigated at each resolution level. Table 1 describes structural features, providing a vocabulary to be used for the results and discussion as important aspects to be studied and understood.

3.2. Density structures of cuticle samples

The scanning of the cuticle samples resulted in large files detailed in Supplementary Table S1 that enclose billions of density voxels in thousands of sections per sample. One can view the data as individual sections, e.g. Fig. 1, in which single sections in the X, Y and Z directions can be viewed simultaneously in appropriate software (e.g. DataViewer or ImageJ with 3D plugin). The DataViewer software allows viewing and subsetting of a current data set as a grey scale of the density as seen in Fig. 1X,Y,Z or as false color rendering of the densities. But also, usefully, DataViewer allowed a rotation of the data structure to a new orthogonal perspective, which allowed optimizing the view of a particular structure, such as in Fig. 1 where adjustment of the Z plane allowed seeing a large field of basal granules, new objects described in Table 1, more clearly. The labeling in view Fig. 1-Z obviates labeling in the thinner perspective of the cuticle seen in views X and Y. The compressed layers seen in cross-section in Fig. 1-X and 1-Y can be seen as much larger in the grazing tangential section seen in Fig. 1-Z in which the traditional layers of the cuticle (epicuticle, exocuticle, endocuticle and membranous layer) are labeled.

DataViewer software allowed assignment of false color lookup tables to voxel densities, which allowed density related structures (e.g. continuations of canals and stalactites between voxel planes) to be recognized more easily within and between serial sections. Once a structure of interest was identified, the entire enclosing mega-structure of voxels was rotated to optimize viewing the structure of interest, and the newly defined voxels were trimmed to contain the structure of interest, then saved with the new rotated coordinate system to a separate file with a reduced voxel count. Several voxel sets were saved using DataViewer as image sections oriented in new XY, XZ, or YZ rotations. These smaller sets of voxels in sections were read into ImageJ and used to extract contours of objects using the ImageJ point selection tool and rendered into 3D visualizations using R. ImageJ also allowed chosen voxel planes to be saved individually in a lossless manner or together into a single AVI file for further storage and analysis. Lossless storage is essential for future measures of density statistics.

3.3. Extracting schematic object distributions from low and high resolution scans

The low resolution file (3.5 μm voxel edge) of sample M2C was small enough, Supplementary Table S1, that some of the objects described in Table 1 could be resolved in the entire set of voxels sampled. The particular objects of interest are recorded in a 3D plot of object outlines in Fig. 2 extracted from the microCT scan of the cuticle sample M2C, pictured in the inset, which has a similar visual orientation as the 3D contour plot. The contour outlines of objects were obtained manually using the multi-point measurement tool of ImageJ. Assigning different colors to each object of interest allowed their distribution in 3D to be viewed as contours plotted in a 3D rotatable graphic space. For a particular object type, e.g. the basal granule, the cluster of points outlining each individual object over several voxel slices were saved in a single CSV file separated from other individual objects by records with the xyz coodinates set to NA. This allowed each object type to be accessed and computations (e.g. the object centroid) to be carried out on the individual objects. In 3.5 μm resolution the objects which could be completely catalogued were pits of organules, stalactites, nipples of organules, and basal granules. The continuity of some structures was difficult to follow from section to section in lower resolution data given their irregular shape, which particularly applied to the Bouligand spirals and dermal canals traveling obliquely. But with appropriate reorientation the 1.5 μm resolution voxel data from sample M3A_1.5 μm allowed Bouligand spirals and dermal canals to be located reliably.

Please cite this article in press as: Kunkel, J.G., et al., 3D-Xray-tomography of American lobster shell-structure. An overview. Fish. Res. (2016), http://dx.doi.org/10.1016/j.fishres.2016.09.028

Table 1
Features revealed in Xray tomography of lobster carapace cuticle medallions. Cuticle layer features are first listed in order outside surface to inside basal surface. Added objects and structures are listed next alphabetically A to Z.

Feature (out to in)	Type	Description
Cuticle surface	plane	The outer surface of the lobster epicuticle facing the environment.
Epicuticle	layer	The epicuticle is a proteinaceous layer, the first to be laid down during the D_1 phase of the molting cycle (Waddy et al., 1995).
Exocuticle	layer	The exocuticle is a chitinous and proteinaceous layer, laid down under the epicuticle as Bouligand layers during the remainder of phase D of the molting cycle prior to actual ecdysis and subsequently mineralized (Waddy et al., 1995), exhibiting substantial mineral incorporation in the Bouligand layers as stalactites.
Ecdysial	plane	The artifact resulting at ecdysis separating the exocuticle, laid down prior to ecdysis, from the endocuticle, laid down after ecdysis.
Endocuticle	layer	Cuticle laid down as Bouligand layers after ecdysis, starting at stage B of the molting process and ending by C_3 (Waddy et al., 1995) and exhibiting substantial mineral incorporation in the Bouligand layers as Bouligand spirals.
Mineral bottom	plane	The apparent bottom of the endocuticle.
Membranous	layer	Bottom of Bouligand layers that has no apparent mineral density but houses mineral objects, the basal granules A non-mineralized layer of cuticle material laid down during C4, the intermolt (Waddy et al., 1995)
Membranous layer bottom	Plane	The bottom of the membranous layer and interface with the epidermis.
Feature (A-Z)	Type	Description
Basal granule	structure new object	Granules with a similar density as the stalactites and Bouligand spirals are embedded in the membranous layer.
Bouligand layers	structure	Bouligand (1972) described the optical illusion of cuticle layers created by rotation of the direction of chitin fibers deposited parallel to the surface plane, characterized more recently as the twisted-plywood structure (Raabe et al., 2006).
Bouligand spiral	new object	Mineral density is associated with the Bouligand layers of the endocuticle from the ecdysial layer to the Bottom of mineral endocuticle as solid relatively uniform densities extending from a central axis in one direction following the Bouligand layer at that level. This results in a pinwheel effect when viewing the frames of an AVI in the direction perpendicular to the surface plane proceeding through the endocuticle.
canal	object	Dermal glands (Talbot and Demers, 1993) and bristles have apatite canals (Kunkel et al., 2012) through which their secretion and nerves are respectively conducted.
mushroom body	new object	This structure is a modified form of stalactite, having the same density but with a more robust outline. It has a stem that occupies the exocuticle similar to a stalactite attached to the calcite layer. However, it protrudes down through the ecdysial plane and mushrooms out to a larger structure only in the endocuticle, usually ending half way through the C4 endocuticle.
nipple	object	Dermal gland- and bristle-canals organules end in a protrusion at the mineral bottom into the membranous layer, which contain phosphatic deposits as demonstrated by EMP ().
pit	object	Dermal gland- and bristle-canal organules open into depressions (pits) in the cuticle surface.
spiral axis	structure new object	Each *Bouligand spiral* is constructed about a central spiral axis which proceeds in the endocuticle from the ecdysial plane toward the epidermal surface but usually terminating before the mineral bottom plane.
stalactite	new object	An elongated structure perpendicular to the surface often an extension of the $CaCO_3$ outer continuous layer of the exocuticle that usually terminates as discrete object type at or above the ecdysial plane but can extend beyond in a few typical ways. A stalactite can also initiate independently below the $CaCO_3$ surface. In general it tapers from its outer to inner extremity.
stalactite axis	new object	The trace of the center a stalactite-cross-section identified using ImageJ in planes of the cuticle parallel to the surface.

The planes separating well defined layers of the cuticle exocuticle, endocuticle and membranous layer were generally identifiable at all resolutions as depicted in Figs. 2,3,5 and 6. Rather than outline all Bouligand spirals, the central axis of the spiral was recorded and followed in adjacent sections and then treated as an object, which allowed the nearest neighbor distances of Bouligand spirals to be computed.

Discrete object centroids were calculated for each object. Then their nearest neighbor distances (NND) to similar objects were calculated and presented as a median NND ± SD(n). The SD is the standard deviation and n is the sample size, Fig. 7. The median was chosen as more representative of the majority of the distances given a skewed distribution. The most distant regular cuticle features are the surface organule pits which need to be characterized in a low resolution sample such as the M2C 3.5 μm data set, Fig. 2, which has enough pits to provide a reasonable sample size. In that large area cuticle M2C 3.5 μm data set, organule pits have a median NND of 189 ± 66(31) μm. The more numerous basal granules had a median NND of 69 ± 30(384) μm determined in the 3.5 μm data set.

The middle abundance structures (stalactites, Bouligand spirals and basal granules) were characterized in smaller cuticle area sections of the higher resolution M2C 0.5 μm sample set, Fig. 5 where stalactites and Bouligand spirals were easier to delineate. As seen in Fig. 7 the basal granules, Bouligand spirals and stalactites had median NNDs that show a decline as one moves from the inner membranous layer basal granules through the endocuticle Bouligand spirals and exocuticle stalactites to the surface pits. The distribution of basal granules in the larger area, 3.5 μm cuticle data set, was similar but distributed significantly broader than that NNDs determined for the smaller area, M2C 0.5 μm cuticle data set.

Please cite this article in press as: Kunkel, J.G., et al., 3D-Xray-tomography of American lobster shell-structure. An overview. Fish. Res. (2016), http://dx.doi.org/10.1016/j.fishres.2016.09.028

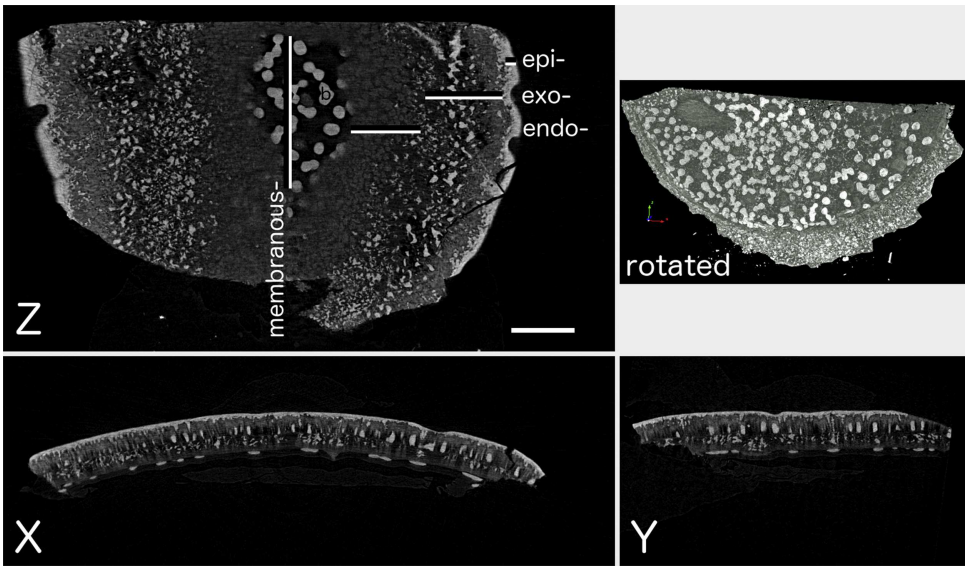

Fig. 1. Cuticle medallion M1C 3.5 μm of American lobster, *Homarus americanus,* data sample. Single orthogonal X-, Y- and Z-plane sections of microCT voxel densities are presented as grey scale images. A select rotated set of the data allowed a section including mainly basal granules as an illustration of the capability of focusing on a particular feature. The horizontal bar in panel Z measures 700 μm (200 voxels at 3.5 μm/voxel-edge data resolution). In the Z panel a cuticle section broadened by tangental view is labeled *epi-*, *exo-*, *endo-*cuticle, and membranous layer and their extents indicated by black/white bars.

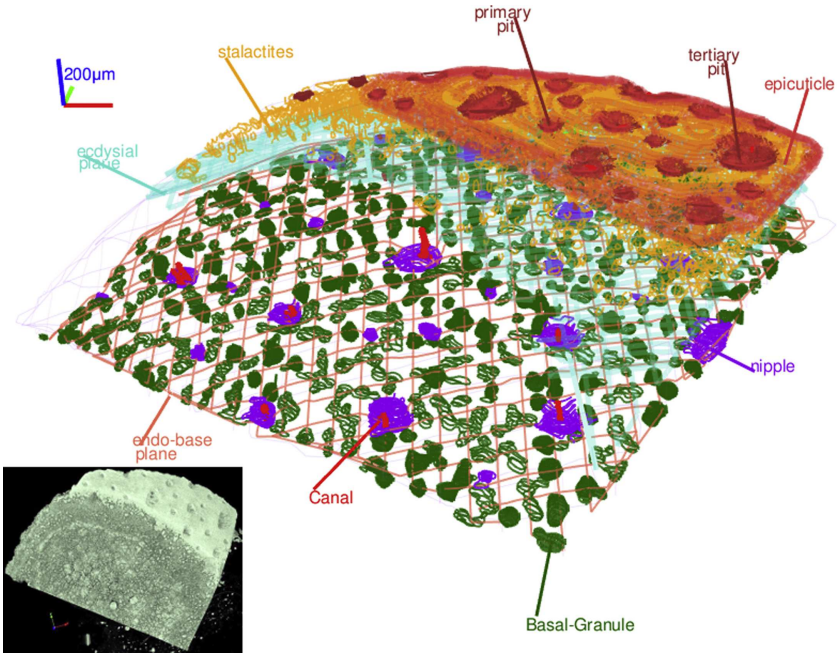

Fig. 2. Cuticle medallion M2C 3.5 μm of American lobster, *Homarus americanus,* shows outlines of objects defined from microCT data. An inserted greyscale LM image of the opaque specimen is included. The 3D contours illustrate the surface plane (orange) and merge into stalactite extensions (orange) into the exocuticle, Surface organule pits are outlined in brown. Dermal canals (red) extend from surface pits (brown) to the endocuticle nipples (purple) but are seen here as terminated in the polished sample oblique cross-sectional surface. The two planes separating the *exo-*, *endo-* and membranous- cuticle are a crosshatched turquoise ecdysial plane and a coral hatched endocuticle base plane. The organule nipples (purple) with attendant canals are seen to depress the endocuticle base plane which is seen as more obvious when rotating in Supplementary videos S1, S4 and S5. Basal granules (dark green) populate the membranous layer. (For interpretation of the references to colour in this figure legend, the reader is referred to the web version of this article.)

At least three size categories of organule pits were recognized as suggested previously (Kunkel and Jecinovic, 2013). Here we found that primary pits were the smallest and always had one glandular canal opening. A primary pit was never seen with an associated bristle. Secondary pits are larger and had two or three canals and one of the canals may have served a bristle. At the two low resolutions, 3.5 μm and 1.5 μm, the number and path of canals was difficult to follow and thus Fig. 2 does not show canals associated with each pit. However the same cuticle specimen M2C scanned at higher resolution, 0.5 μm, allowed the number and paths of canals to be detailed, Figs. 5 and 6. Tertiary/Quarternary pits were seen to have up to five canals, one or more of which served a bristle. In gen-

Please cite this article in press as: Kunkel, J.G., et al., 3D-Xray-tomography of American lobster shell-structure. An overview. Fish. Res. (2016), http://dx.doi.org/10.1016/j.fishres.2016.09.028

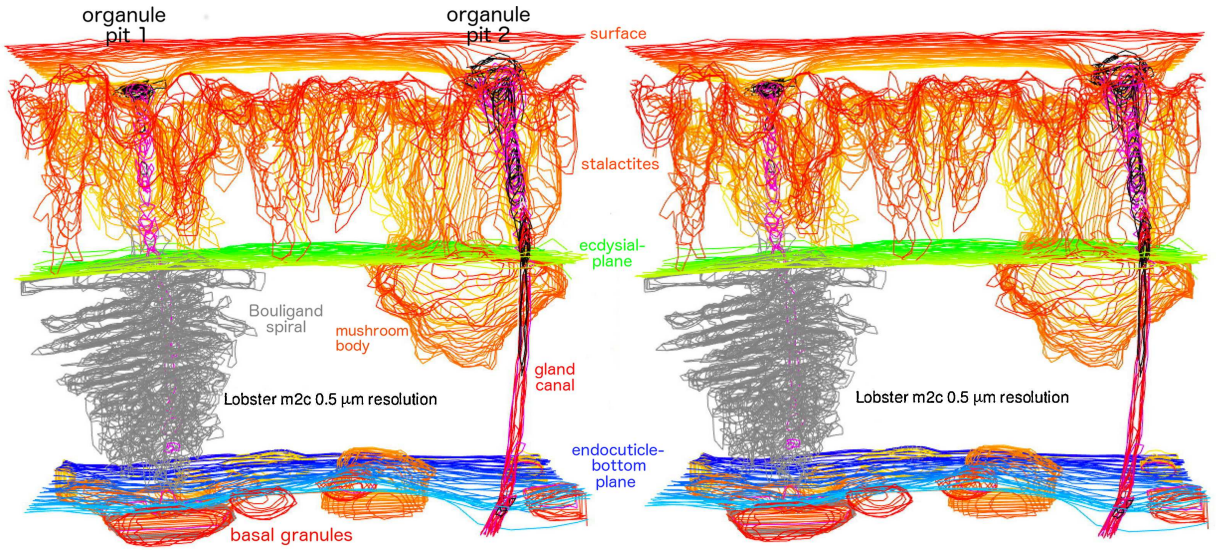

Fig. 3. A stereo pair of outlines derived from American lobster, *Homarus americanus,* cuticle medallion (M2C 0.5 μm voxel resolution) microCT data using ImageJ, can be viewed in stereo if you cross your eyes to merge the two images or use a stereo viewer. Two organule pits are seen as depressions in surrounding plain cuticle. The surface, stalactites and basal granules are presented (shades of orange-yellow) in receding tones for perspective. The ecdysial plane (shades of green) separates the exocuticle from the endocuticle. A mineral endocuticle bottom plane (shades of blue) overlays the membranous layer which houses embedded basal granules. One Bouligand spiral (grey) is displayed. Dermal gland canals (violet). In stereo-view one can see the arrangement of stalactites surrounding and between the two primary organule canals. This figure also shows one of the occasional Bouligand spirals that actually surround a dermal canal. A set of stereo images of this same file is available as Supplementary Fig. S3 which provide perspectives from above and below the ecdysial plane allowing the spiral path of the Bouligand spiral to be appreciated. (For interpretation of the references to colour in this figure legend, the reader is referred to the web version of this article.)

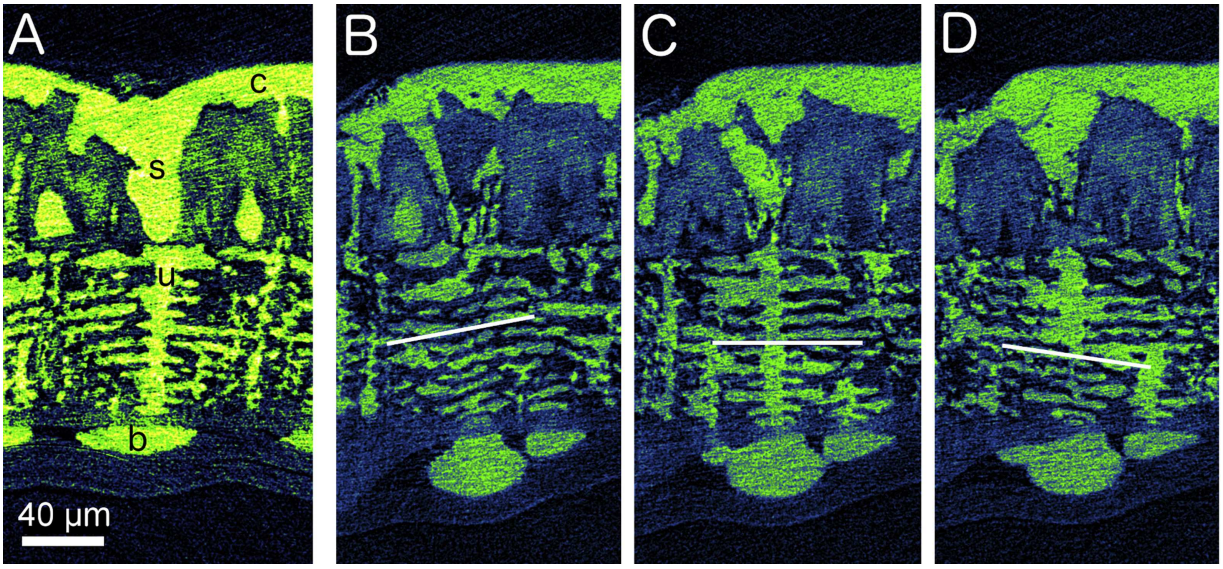

Fig. 4. American lobster, *Homarus americanus,* medallion (M2C 0.5 μm voxel resolution) raw data sections demonstrate an axial alignment of stalactites, Bouligand spiral, and basal granules oriented perpendicular to the cuticle surface's calcite layer. A. One stalactite-Bouligand spiral-basal granule, s-u-b, voxel plane is close to its longitudinal axis. The calcite, c, of the surface epicuticle layer is seen to be continuous with the stalactite, s, Bouligand spiral, u and basal granule, b densities. B,C,D. A second example of a stalactite-Bouligand spiral-basal granule voxel section focused on the spiral's central axis is visualized at C, and several sections away on either side of the center, B and D. White lines indicate the angle of the cuticle's Bouligand spiral and Bouligand layer mineralization. Note that the stack of Bouligand layers in C is perpendicular and connected to a mineralized core axis and the angle of the Bouligand layer is reversed in B and D as would be expected for a helicoid spiral. A 40 μm bar in the lower left of panel A serves all four panels.

eral, in the carapace cuticle all canals connected to a cuticle surface pit and all pits had one or more canals connected to the pit bottom. A cuticulin defined pit is associated with all carapace organules.

3.4. Objects at higher resolution

Subsets of data from the high resolution (0.5 μm/voxel) scan of sample M2C include three cropped sets that focused on three tentative grades of organules: primary, secondary and tertiary. Fig. 3 is a stereo pair with object contours surrounding two primary organules. It includes the cuticle surface, ecdysial and endocuticle bottom planes, two dermal gland canals with their associated pits, plus surrounding stalactites, one Bouligand spiral and several basal granules. In this case a single depicted Bouligand spiral is deployed around one of the canals. That was not the typical relationship. Bouligand spirals most often were seen starting at the ecdysial plane, *e.g.* at the termination of a stalactite as seen in raw form in Fig. 4A. Another atypical structure observed in this figure

Please cite this article in press as: Kunkel, J.G., et al., 3D-Xray-tomography of American lobster shell-structure. An overview. Fish. Res. (2016), http://dx.doi.org/10.1016/j.fishres.2016.09.028

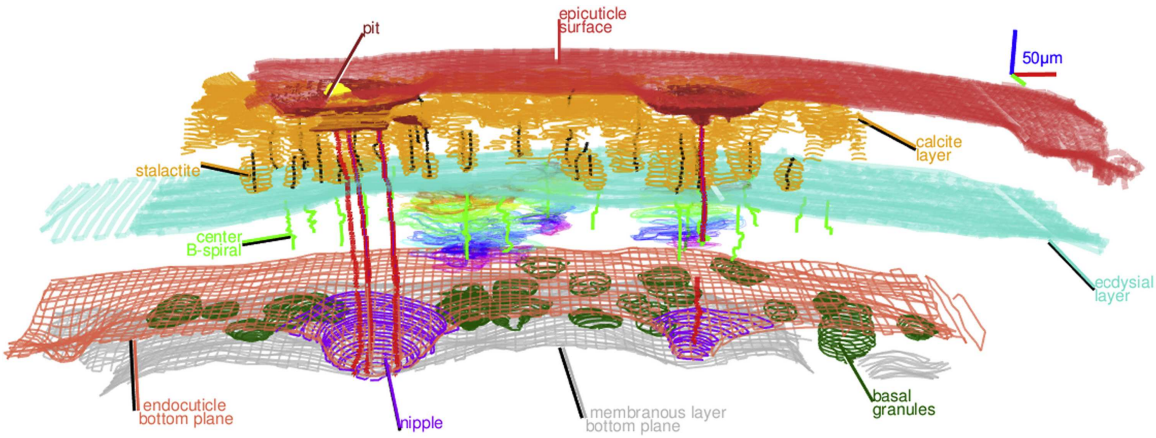

Fig. 5. American lobster, *Homarus americanus,* medallion (M2C 0.5 μm voxel resolution) object contours. One primary organule with one canal and one secondary/tertiary organule with 3 canals (red), one hosting a bristle (yellow) and surrounding cuticle structures embedded in particular cuticle layers. Epicuticle surface (red), organule pits (brown), calcite layer and stalactites (orange) and basal granules (dark green). Ecdysial layer (turquoise). Mineral endocuticle bottom (coral). Membranous layer bottom (grey). Three Bouligand spirals (in rainbow colors) and all other spiral axes (green) are depicted. Canals (red). A video rotating this structure is available as Supplementary file S4. (For interpretation of the references to colour in this figure legend, the reader is referred to the web version of this article.)

is the extension of a stalactite into a mushroom body (Table 1), whereas the typical extension of a stalactite is a Bouligand spiral in these samples or an early termination without an extension. Fig. 3 is a stereo pair viewed from slightly above the ecdysial plane. From that perspective in the figure one can see along and through several outlines of the Bouligand spiral on its left that show a spiraling down and around to be continuous with the Bouligand spiral outlines on the right. The Bouligand spiral effect is further seen in Fig. 5 where sequential planes of density are given a rainbow series of color in a spiral. The spiral is also visible in the Supplementary video, Fig. S2, of raw voxel frames viewed along the axis of the spiral in which the $CaCO_3$ density voxels are seen as the leaves of a fan rotating in concert with the Bouligand layers of the cuticle as one proceeds down the spiral.

Another way to visualize the spiral effect is in longitudinal transects of the Bouligand spirals in planes cutting the spiral along its long axis and visualizing the middle plane and in parallel planes preceding and following a middle transect, e.g. Fig. 4A or C. A better orientation was accomplished by rotating the density file using the Dataviewer software so that the stalactites and Bouligand spirals are correctly perpendicular to the shell surface. With that reorientation, in Fig. 4A the calcite surface layer is seen to be directly connected to a stalactite, which is connected at the ecdysial plane to a Bouligand spiral, which tapers down to apparently contact a basal granule. The structure of the spiral is elucidated in panels 4B-D. The direction of the spiral's gyre and continuity of the spiral is only revealed by viewing sections prior to and following the axial plane. The direction of the spiral gyre indicated by the superimposed white line in the figures is tilted oppositely on the two sides, panes B and D, but appears level in the central transect pane C.

Two different organules are presented in Fig. 5, one a primary and the other a secondary organule with three canals, one canal serving a bristle. Fragments of other organules are visible in the periphery on either end of this assemblage. It is necessary to see the canal structures serving the pit in order to properly classify the actual complexity of an organule. The continuity of the canal in the primary organule of Fig. 5 is seen to be interrupted which can happen when the resolution in particular adjacent slices makes it difficult to follow the continuity. Continuity is usually best followed from either surface and may become difficult in the middle slices as seen in this example. This may be an indication that the freeze-substitution fixation used may not be effective in preserving some central layer detail of the cuticle.

Two views of the same tertiary organule are seen in Fig. 6, one a false color interpretation of a density voxel tangental slice through the endocuticle nipple, Fig. 6A, of the organule showing the 5 canals as seen at that level and the second panel, Fig. 6B, outlining the objects of interest in a 3D contour depiction of the tertiary organule *epi-*, *exo-*, *endo-* and membranous-cuticle structure. Of interest is the ability to differentiate between the canals including the ability to identify the bristle bearing unit, canal 1, and amorphous secretion coming out of canal 4. The identity of canal 4 as the source of the secretion requires looking at the structure rotating in Supplementary video, Fig. S5. Another feature not included in the 3D contour false-color interpretation is that three of the canals appeared empty (i.e. X-ray translucent) while the other two, canals 3 and 5, are filled with an X-ray dense material for a substantial portion of their length. It is clear that the 0.5 μm microCT resolution is needed to characterize the canal contents along their entire lengths. In Fig. 6B organule data set another feature of note is a section profile of a tear shaped basal granule, visible on the left face of Fig. 6, which shows the basal granule tear apex depressing the basal plane of the membranous layer. This is also seen more clearly when one observes the AVI video, Supplementary Fig. S5, of the organule data set. Fig. 6 also exhibits another example of the occurrence of the mushroom body (Table 1) extension of a stalactite type object which happens often associated with an organule.

4. Discussion

Using microCT we have identified the arrangements of the mineral densities in lobster carapace cuticle as traditionally understood structures as well as novel objects that had not previously been seen. These arrangements have substantial significance for the recent attempts to characterize the lobster cuticle as a composite material with uniform ordered properties, but also provides potential insight into the stages of cuticle deposition and renewal, as well as the pattern of developing shell disease, which attacks the lobster carapace in a pattern consistent with objects described here. We studied exclusively the intermolt, C4 stage, of American lobster, which should have all the structures that occur in the final carapace cuticular structure before the start of the cuticle replacement and molting process (Roer and Dillaman, 1984). The stalactites, Bouligand spirals and basal granule objects are found in all three intermolt lobsters studied here but it is not known how general and constant a character set they represent as the cuticle develops and under different environmental pressures. The status of these new

Please cite this article in press as: Kunkel, J.G., et al., 3D-Xray-tomography of American lobster shell-structure. An overview. Fish. Res. (2016), http://dx.doi.org/10.1016/j.fishres.2016.09.028

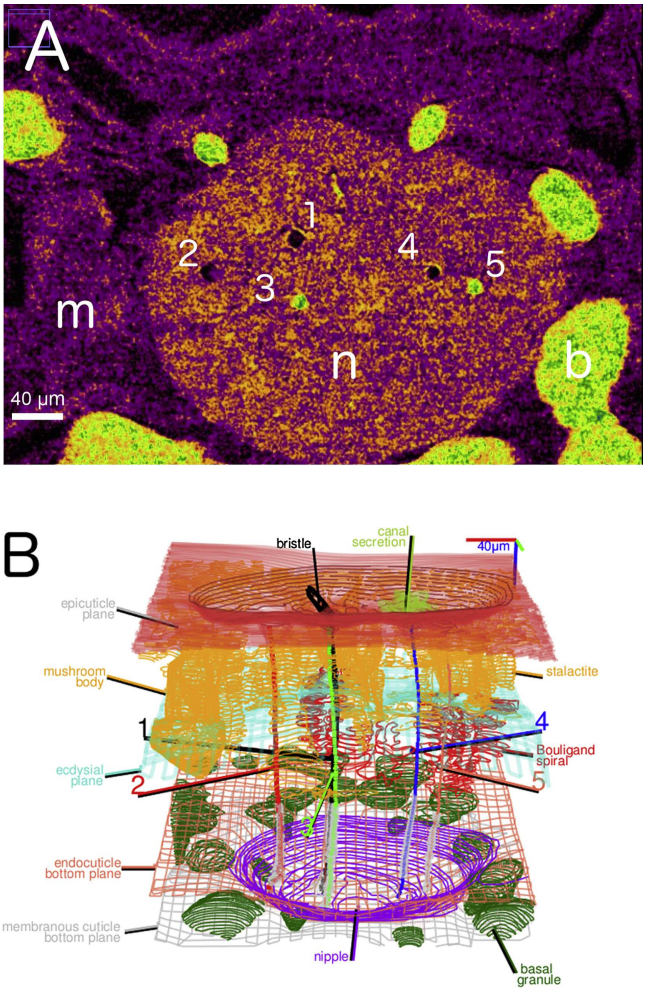

Fig. 6. American lobster, *Homarus americanus*, cuticle medallion (M2C 0.5 μm voxel resolution) single tertiary/quarternary organule outlines. Two views of the same organule showing its 5 canals. A. Density voxel tangental section through the membranous layer, m, containing an endocuticle nipple, n, with five dermal canal profiles labeled 1–5 and several basal granules, b, in the surrounding membranous layer. Canal #1 leads to the bristle seen in B and its canal appears to be empty. Canals #2 and #4 are also largely empty. Canals #3 and #5 are filled with an unknown substance of similar density as the basal granules. A horizontal white bar in lower left indicates 40 μm. B. Plot of the object contours for this tertiary/quarternary organule. Several planes are schematically depicted by contour lines and named from outside to in: the epicuticle outer surface (red), the ecdysial plane (turquoise), the endocuticle base plane (coral) and the membranous layer base-plane (grey). Within these layers are distributed the components of the organule starting with the 320 μm diameter pit encompassing the 5 canals. Surrounding the organule extending down from the calcite layer (orange) are the orange stalactites one of which is expanded beyond the ecdysial plane as a mushroom body. The five canals end in a phosphate rich nipple structure (purple) which depresses the endocuticle bottom plane intruding into the membranous layer. Within the membranous layer are found the basal granules (dark green) which are in some cases extended into teardrop shapes which depress the membranous cuticle bottom plane. Outlines of several Bouligand spirals (red) are evident in the endocuticle layer. A video rotating this structure is available as Supplementary file S5. (For interpretation of the references to colour in this figure legend, the reader is referred to the web version of this article.)

exoskeleton structures will be of interest during the molt and intermolt cycle and will potentially help us understand the development and function of the lobster cuticle, the potential effects of ocean acidification, consequences of lobster storage and the development of various shell diseases.

The border between the epicuticle and exocuticle is not well differentiated with microCT in our current study. In arthropods the epicuticle originates as the cuticulin layer, a protein layer devoid of chitin lamellae (Locke, 1969), and invested with protective organic compounds including waxes and lipids providing a protective barrier from the environment. Exactly how the epicuticle is composed in the crustacea has not been generally well described, but it has several proteins specific to it (Kunkel, 2013). Using microscopes based on other physical principles the epicuticle is seen to be invested with well oriented calcite (polarized light microscope, Kunkel et al., 2012). The calcite layer of the lobster epicuticle hosts apparently collapsed pore canals (AFM, Kunkel, 2013) when compare with the ovate-crescent like pore canals of the *exo*-and endocuticle and has a higher density profile of calcium and magnesium and an absence of phosphate (EMP, Kunkel et al., 2012; Kunkel and Jercinovic, 2013). The collapse of the pore canals is likely the result of forces created by the growing calcite crystal which comes to dominate the density and thickness of this only cuticle layer devoid of chitin. These properties are not evident here in the microCT view of the epicuticle and in its transition to the exocuticle. There does not seem to be an obvious density transition between what should be a calcite layer of the epicuticle and the attached stalactites as seen in Fig. 4.

Stalactites, Bouligand spirals and basal granules are described here as new objects and are arranged in series occupying respectively the inner exocuticle, the mineral endocuticle and the membranous layer of the intermolt stage, C4, lobster dorsal lateral carapace. The dorsal lateral carapace cuticle is perhaps the largest expanse of cuticle uncomplicated by arthropod joints, muscle attachments and membranes and is a likely cuticle structure that may be able to be understood from an *ab initio* modeling perspective (Nikolov et al., 2011). It is also a key structure aside from the chela base that is used in the field to characterize the lobster's stage of molting cycle (Waddy et al., 1995). MicroCT will be invaluable to follow both the genesis of the C4 cuticle structures and their dysgenesis during the D-series of stages underlying the approach to molting (Waddy et al., 1995). Based on their density and connectivity the stalactites, Bouligand spirals and basal granules all are likely composed primarily of $CaCO_3$; however that composition needs to be established given that this is their first description as discrete objects. Most of these new objects have multi-μm diameters, and now that their distribution can be described with the non-destructive microCT, correlative microscopy should allow us to analyze their chemical properties where the 3-D structure extends to a revealed polished surface. The ability of microCT to be done on multiple samples over-night will allow various chosen polishing angles to be applied, and after microCT to choose appropriate polished structures for hi-res SEM, EMP, FTIR spectroscopy, AFM and Raman spectroscopy which should allow their chemistry to be confirmed and explored during their development.

The properties of carapace objects are of theoretical and practical interest. Compositional transects of the calcite, exocuticle, endocuticle and membranous layers have been reported earlier (Kunkel et al., 2012; Kunkel and Jercinovic 2013). Those studies quantified the Ca, P, Mg, Cl, F, Sr, Mn, and Ba at one micron resolution in transects of the cuticle layers. The transect paths passed through the then recognized structures of the cuticle, showing substantial variation quantified by EMP in the exocuticle and endocuticle, particularly with respect to phosphate which might be explained by new objects described here. However, this must be corroborated by further study in which 3-D objects of interest, identified by microCT are analyzed by 2D methodologies at polished surfaces.

The spacing of cuticular objects is in many cases over-disperse, tending toward hexagonal closest packing *i.e.* close to even spacing. This is true for the carapace surface pits which have the widest spacings of regular cuticle structures as well as for stalactites, Bouligand spirals and basal granules. This distribution of stalactites, Bouligand spirals and basal granules, based on their nearest neighbor distances may correspond to their being produced one-for-one

Please cite this article in press as: Kunkel, J.G., et al., 3D-Xray-tomography of American lobster shell-structure. An overview. Fish. Res. (2016), http://dx.doi.org/10.1016/j.fishres.2016.09.028

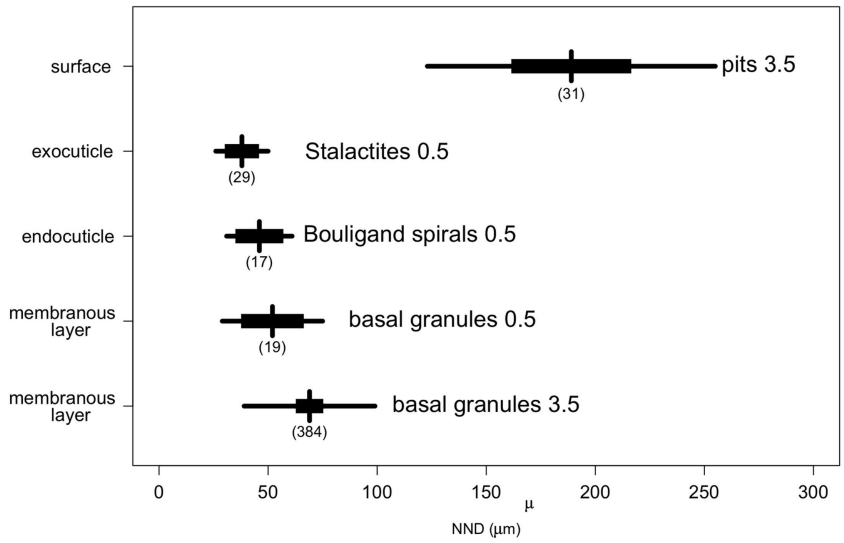

Fig. 7. Comparison of nearest neighbor distances (NND) between similar objects in American lobster, *Homarus americanus* cuticle samples. Distances between objects were measured in micrometers (μm) in the M2C 0.5 μm resolution (labeled 0.5) or the M2C 3.5 μm resolution (labeled 3.5) samples (Table S1). The median NND is plotted vs its basal to surface layer in the cuticle. One standard deviation of the distances about the median is indicated by the thin line, while the thicker line with square ends represents a 95% CI of the mean.

by underlying epidermal cells including the socket-producing and canal-producing cells of organules as suggested from Fig. 4BCD. Thus the spacing of the stalactites, Bouligand spirals and any associated basal granule may well be tied to the approximate hexagonal closest spacing of typical epidermal epithelia. On the other hand, the spacing of organules, with a NND of ~200 μm, separated by several pavement epidermal cells, may need to be regulated, not physically but rather by short range growth regulator substances which have been theorized to control epidermal organule development in general (Merritt, 2006).

This is the most detailed description of carapace organules in lobsters. Theoretically, lobster organules develop from single epidermal cells (each of which is a potential organule stem cell, Henke, 1952; Lawrence, 1973) but the presence of organules nearby will inhibit close surrounding epidermal cells from developing toward an organule. When, due to isometric growth of the lobster epidermis through growth and molting, the existing organules are separated by enough distance to reduce the organule-growth-regulatory-substances to a low enough titer, a new organule will be induced in the cell nearest the center of that lowered titer. The newly induced organule will be a primary organule in our current model of organule birth and development. This basic pattern of development, though well supported in theory (Turring, 1952; Murray, 2003), has yet to be validated for arthropod organule pattern by modern cell or molecular biology. The actual development of different classes of organules is not entirely clear yet. In the organules illustrated in Figs. 3, 5, and 6 the observed number of canals per pit proceeds from 1 to 3 to 5 which could suggest a mechanism, but if examples of 2 and 4 canals per pit surface with further study, the number of alternate mechanisms may increase. Here is one proposal of a mechanism: The function of the fourth cell, the *neben zell* of Henke (1952), of the primary organule actually serves as a further organule stem cell, then proceeding from one to two canals might be the more logical progression ... the organule stem cell produces an accessory organule, then this secondary organule (with two canals and now with two stem cells), could proceed in a future molting cycle to a three or four canal more advanced organule and theoretically in another cycle to a five or more canal organule. Such theories could be pursued by observing the actual frequencies of organule types during development and applying mathematical simulations to how those frequencies might be established. This simulation is important for instance in demonstrating that the tertiary/quarternary organules are not a simple coincidence or randomly generated primary organules.

Classifying each organule pit superficially with a dissecting or compound LM is often obscured by secretions or microbial films in the pits. Current microCT provides the resolution at about the same resolution limit as the LM (~0.3 μm) but with 3D voxels allowing one to see beyond surface films to the differential density of the shell structure. Thus the microCT approach to organule classification allows observation of organule spatial distribution and classification as primary, secondary, and further. It is not clear if there is an end to this sequence of elaborating carapace organule structures given the continued growth by molting of adult American lobsters but in the wide size range of lobsters we have observed so far we have only seen 3 or 4 size classes of carapace pits. Details of this development will be of interest in comparing the American lobster organules with those of its congener, the European lobster *Homarus gammarus*, whose carapace and claw organules are described as different structurally and in distribution using LM and SEM (Davies et al., 2014). The functions of the lobster carapace organules are not well understood, or even studied, perhaps because the majority of study of organules has concentrated on the more elaborate set of sensory setae functions on antennae, mouthparts, dactyls and terminal segments of arthropods (e.g. Lavalli and Factor, 1992), which relate them to more easily studied neurosensory responses such as chemosensory and tactile signal or integrated into an understandable response such as an orientation or escape reflex.

The resolution of microCT at this stage does not allow us to resolve some objects of interest such as cuticle pore canals, which are resolved better morphologically in 2D by EM, SEM e.g. (Fabritius et al., 2009) and AFM (Kunkel, 2013) but the advantage of an inventory of the resolvable objects and their relationships in 3D creates an improved understanding of cuticle organization. Some analysis of the relationship of shell objects will require custom R-scripts to automatically access the centroids of identified objects and calculate the average and variance of the density of each object type, as well as any changes along the length or expanse of structures. Further analysis should also include chemical and biochemical analysis of the new objects discovered. Their locations in cuticle fragments with achievable polished surfaces are now able to be

Please cite this article in press as: Kunkel, J.G., et al., 3D-Xray-tomography of American lobster shell-structure. An overview. Fish. Res. (2016), http://dx.doi.org/10.1016/j.fishres.2016.09.028

known and their dimensions are within the resolution of 2D analytical techniques. Of particular interest would be the substructure of the early epicuticle which includes a thin cuticulin layer which establishes the sculpturing of the resultant cuticle surface but is typically 18 μm in thickness, which is well below the current resolution of microCT. The surface shape of the organule pits and the remainder of the cuticle surface are determined by the cuticulin layer (Neville, 1965; Locke, 1966) including many ornate structures that form non-sensory spines and frills associated with the arthropod cuticle surface. Many of these sculpturing details are produced by epidermal cells modeling their cuticulin layer. However, arthropod epidermis has evolved a special epidermal developmental diversification path, the organule, which allows epidermal cells to differentiate from the generalized epidermal cell type into gland and sensory structures. These structures derive from a single epidermal cell and differentiate into a small number of cell types and cells, typically four cell types, which is why they were given the diminutive name, organule (Lawrence, 1973; Merritt, 2006). Two of the organule cell types, the socket and the canal cell, perform familiar epidermal cell functions, producing a cuticulin layer, which creates the specialized surface sculpturing of the organule pits, bristles and canals. The detail of that sculpturing and how it overlays the calcite layer of the general cuticle and apatite lining of the canals provides multiple opportunities for structural vulnerabilities to develop.

The theory of arthropod organule development and spacing is similar to that of mammalian skin follicle spacing (Claxton, 1964) in which necessary new hair follicles develop evenly spaced in a collagenous matrix as the keratinaceous skin layer isometrically expands during the more continuous growth exhibited by vertebrates. Recent work in mice has identified genes associated with the even spacing of hair follicles and link it to a reaction diffusion mechanism (Sick et al., 2006; Stark et al., 2007), similar to that suggested for arthropod organule spacing (Lawrence, 1973). This formation of organules in arthropod epidermal development results in structures that function as glands (called tegumentary glands in crustaceans, e.g. Talbot and Demers (1993)) or sensory organs which have varied forms in Decapods (Garm, 2004). The variety of organule structures may be as numerous as the variety of species of arthropods. Carapace cuticle organules described above, in Figs. 1–7, are a model of organule generation that may be able to be understood, and exemplify how secondary and tertiary organules develop. Their existence inserted into a plane of ordinary epidermal cells allows them to be studied somewhat in isolation compared to the crowded assemblage of organule types found on the linear appendages such as antennae, antenules, mouth parts or swimmeretes (Killian and Page, 1992). The carapace organules although of yet unknown function, vastly outnumber the previously described glands and sensory elements of lobster's linear structures on the lobster exoskeleton. If the nearest neighbor distance NND of carapace organules is ~200 μm, a commercially legal lobster with ~83 mm carapace length would accommodate approximately 450,000 carapace organules. Similarly spaced organules are found on the chelae and all the dorsal sclerite surfaces of the remaining lobster exoskeleton, a similar or larger area compared to the carapace (and places where ESD develops in severe cases), providing surface for a net million similarly constructed and spaced organules. On the other hand, the numbers of each type of specialized organule on linear structures such as swimmeret margins, antenna, antennules are rather in the hundreds or low thousands. Indeed, the potential role of the carapace organules in all types of shell disease vulnerability argues for attention going forward to their development and function.

This study used non-proprietary software and custom R-scripts by the authors, freely available to all researchers. It is reassuring that substantial future progress may be made using investigator designed open source analytical tools. The ImageJ open source array of software with its many plugins provides additional avenues of yet unevaluated approaches for analyzing lobster microCT data (Doube et al., 2010). In addition, there exists various commercial proprietary software developed by and for medical research and analysis that is currently available. Such closed-source software performs additional processing and analytic calculations on large tomography data files, and may be found useful for applied research on lobster material if it performs useful diagnostic output, despite not sharing its code. Basic research is needed to define measurable properties of lobster cuticle which may be useful in managing population size and health.

Acknowledgements

The research associated with this project was supported by NOAA grant NA06NMF4720100 to RI SeaGrant supporting the New England Lobster Research Initiative.

Appendix A. Supplementary data

Supplementary data associated with this article can be found, in the online version, at http://dx.doi.org/10.1016/j.fishres.2016.09.028.

References

Andersen, S.O., 2010. Insect cuticular sclerotization: a review. Insect Biochem. Mol. Biol. 40, 166–178.
Bouligand, Y., 1972. Twisted fibrous arrangements in biological materials and cholesteric mesophases. Tissue Cell 4, 189–217.
Clark, P.J., Evans, F.C., 1954. Distance to nearest neighbor as a measure of spatial relations in populations. Ecology 35 (4), 445–453.
Claxton, J.H., 1964. The determination of patterns with special reference to that of the central primary skin follicles in sheep. J. Theor. Biol. 7, 302–317.
Davies, C.E., Whitten, M.M., Kim, A., Wootton, E.C., Maffeis, T.G., Tlusty, M., Vogan, C.L., Rowley, A.F., 2014. A comparison of the structure of American (*Homarus americanus*) and European (*Homarus gammarus*) lobster cuticle with particular reference to shell disease susceptibility. J. Invertebr. Pathol. 117, 33–41.
Doube, M., Kłosowski, M.M., Arganda-Carreras, I., Cordeliéres, F., Dougherty, R.P., Jackson, J., Schmid, B., Hutchinson, J.R., Shefelbine, S.J., 2010. BoneJ: free and extensible bone image analysis in ImageJ. Bone 47, 1076–1079.
Fabritius, H.O., Sachs, C., Romano, P., Raabe, D., 2009. Influence of structural principles on the mechanics of a biological fiber-Based composite material with hierarchical organization: the exoskeleton of the lobster *Homarus americanus*. Adv. Mater. 21, 391–400.
Garm, A., 2004. Revising the definition of the crustacean seta and setal classification systems based on examinations of the mouthpart setae of seven species of decapods. Zool. J. Linn. Soc. 142, 233–252.
Glenn, R.P., Pugh, T.L., 2006. Epizootic shell disease in American lobster (Homarus americanus) in Massachusetts coastal waters: interactions of temperature, maturity, and intermolt duration, J. Crustacean Biology 26 (4), 639–645.
Grunenfelder, L.K., Herrera, S., Kisailus, D., 2014. Crustacean-Derived biomimetic components and nanostructured composites. Small 10 (16), 3207–3232.
Hayes, D.K., Armstrong, W.D., 1961. The distribution of mineral material in the calcified carapace and claw shell of the American lobster Homarus americanus, evaluated by means of microroentgenograms. Bio Bull. 121, 307–315.
Henke, K., 1952. Über zelldifferenzierung im integument der insekten und ihre bedingungen. J. Embryol. Exp. Morphol. 1, 217–226.
Killian, K.A., Page, C.H., 1992. Mechanosensory afferents innervating the swimmerets of the lobster. J. Comp. Physiol. A 170 (4), 491–500.
Kunkel, J.G., Jercinovic, M.J., 2013. Carbonate apatite formulation in cuticle structure adds resistance to microbial attack for American lobster. Mar. Biol. Res. 9 (1), 27–34.
Kunkel, J.G., Jercinovic, M.J., Callaham, D.A., Smolowitz, R., Tlusty, M., 2005. Electron microprobe measurement of mineralization of american lobster, homarus americanus, cuticle: proof of concept. Lobster Shell Disease Workshop, UMass Boston In: New England Aquarium. Aquatic Forum Series, 2005, pp. 76–82.
Kunkel, J.G., Nagel, W., Jercinovic, M.J., 2012. Mineral fine structure of the american lobster cuticle. J. Shellfish Res. 31 (2), 515–526.
Kunkel, J.G., 2013. Modeling the calcium and phosphate mineralization of american lobster cuticle. Can. J. Fish. Aquat. Sci. 70 (11), 1601–1611.
Lavalli, K.L., Factor, J.R., 1992. Functional morphology of the mouthparts of juvenile lobsters, Homarus americanus (Decapoda: nephropidae), and comparison with the larval stages. J. Crustacean Biol. 12, 467–510.
Lawrence, P.A., 1973. The development of spatial patterns in integument of insects. In: Counce, S.J., Waddington, C.H. (Eds.), Developmental Systems: Insects, vol. 2. Academic Press, New York, pp. 157–209.

Please cite this article in press as: Kunkel, J.G., et al., 3D-Xray-tomography of American lobster shell-structure. An overview. Fish. Res. (2016), http://dx.doi.org/10.1016/j.fishres.2016.09.028

Locke, M., 1966. The structure and formation of the cuticulin layer in the epicuticle of an insect, *Calpodes ethlius* (Lepidoptera, Hesperiidae). J. Morphol. 118 (4), 461–494.
Locke, M., 1969. The structure of an epidermal cell during the development of the protein epicuticle and the uptake of molting fluid in an insect. J. Morph. 127, 7–39.
Lowenstam, H.A., Weiner, S., 1989. On Biomineralization. Oxford U Press, pp. 336.
Lowenstam, H.A., 1981. Minerals formed by organisms. Science 211, 1126–1131.
Merritt, D.J., 2006. The organule concept of insect sense organs: sensory transduction and organule evolution. Adv. Insect Physiol. 33, 192–241.
Murray, J.D., 2003. Mathematical Biology. II: Spatial Models and Biomedical Applications, 3rd ed. Springer Interdisciplinary Applied Mathematics.
Naleway, S.E., Taylor, J.R.A., Porter, M.M., Meyers, M.A., McKittrick, J., 2016. Structure and mechanical properties of selected protective systems in marine organisms. Mater. Sci. Eng. C 59 (1), 1143–1167.
Neville, 1965. Chitin lamellogenesis in locust cuticle. J Cell Sci. S3–S106, 269–286.
Nikolov, S., Fabritius, H., Petrov, M., Friák, M., Lymperakis, L., Sachs, C., Raabe, D., Neugebauer, J., 2011. Robustness and optimal use of design principles of arthropod exoskeletons studied by ab initio-based multiscale simulations. J. Mech. Behav. Biomed. Mater. 4 (2), 129–145.
Raabe, D., Romano, P., Sachs, C., Fabritius Al-Sawalmih, H.A., Yi, S.B., Servos, G., Hartwig, H.G., 2006. Microstructure and crystallographic texture of the chitin–protein network in the biological composite material of the exoskeleton of the lobster Homarus americanus. Mater. Sci. Eng. A 421, 143–153.
Richards, A.G., 1951. Integument of Arthropods. University of Minnesota Press, pp. 428pp.
Roer, R.D., Dillaman, R.M., 1984. The structure and calcification of the crustacean cuticle. Am. Zool. 24, 893–909.
Romano, P., Fabritius, H., Raabe, D., 2007. Exoskeleton of the lobster *Homarus americanus* as an example of a smart anisotropic biological material. Acta Biomater. 3 (3), 301–309.
Sick, S., Reinker, S., Timmer, J., Schlake, T., 2006. WNT and DKK determine hair follicle spacing through a reaction-diffusion mechanism. Science 314, 1447–1450.
Smolowitz, R., Chistoserdov, A.Y., Hsu, A., 2005. A description of the pathology of epizootic shell disease in the American lobster, *Homarus americanus* H. Milne Edwards 1837. J. Shellfish Res. 24, 49–756.
Stark, J., Andl, T., Millar, S.E., 2007. Hairy math: insights into hair-Follicle spacing and orientation. Cell 128 (1), 17–20.
Talbot, P., Demers, D., 1993. Tegumental glands of crustacea. In: Horst, M.N., Freeman, J.A. (Eds.), The Crustacean Integument. Academic Press, pp. 151–192.
Tarsitano, S.F., Lavalli, K.L., Horne, F., Spanier, E., 2006. The constructional properties of the exoskeleton of homarid, scyllarid, and palinurid lobsters. Hydrobiologia 557, 9–20.
Turring, A.M., 1952. The chemical basis of morphogenesis. Phil. Trans. R. Soc. Lond. B 237, 37–72.
Waddy, S.L., Aiken, D.E., de Kleijn, D.P.V., 1995. Control of growth and reproduction. In: Factor, J.R. (Ed.), Biology of the Lobster, Homarus Americanus. Academic Press, pp. 217–266.

Please cite this article in press as: Kunkel, J.G., et al., 3D-Xray-tomography of American lobster shell-structure. An overview. Fish. Res. (2016), http://dx.doi.org/10.1016/j.fishres.2016.09.028